First Principle Investigations on Electronic, Magnetic, Thermodynamic, and Transport Properties of $TlGdX_2$ (X = S, Se, Te)

R. Gautam, A. Kumar and R.P. Singh*
Department of Physics, S.S.V. College, Hapur, C.C.S. University, Meerut U.P., India

(Received February 26, 2017; in final form June 17, 2017)

In the present research paper, we investigated spin polarized electronic, magnetic, thermodynamic, and transport properties of thallium gadolinium dichalcogenides $TlGdX_2$ (X = S, Se, Te) using density functional theory. Electronic structure reveals that all the three compounds are wide band gap semiconductors which are beneficial for good thermoelectric performance. Calculated magnetic moment of $TlGdX_2$ is found to be in good agreement with available experimental values and mainly dominant by Gd^{3+} ions. Semiclassical Boltzmann transport theory has been used to calculate the Seebeck coefficient and electrical conductivity for the proposed dichalcogenides. Calculated values of the Seebeck coefficient and electrical conductivity are found to be consistent with available experimental values in literature. Thermodynamic properties of $TlGdX_2$ have also been estimated for the first time and explained on the basic facts.

DOI: 10.12693/APhysPolA.132.1371

PACS/topics: semiconductors, electronic structure, magnetic properties and thermodynamic properties

1. Introduction

Magnetic semiconductors are the compounds that exhibit both the semiconducting as well as magnetic character. These type of materials offer novel functionalities to spintronics and magneto-electronic devices, viz. they can act as spin-filter materials. These materials are used in magnetic tunnel junctions in which magnetic electrodes are separated by an insulating barrier and ballistic transport achieved through the tunneling of the electrons via the barrier [1, 2]. Thallium gadolinium dichalcogenides $TlGdX_2$ (X = S, Se, Te) may be considered as magnetic semiconductors because they consist of magnetic and semiconducting properties. Along with this, they can be assumed as good thermoelectric materials due to their high Seebeck coefficient and thermoelectric figure of merit [3]. Therefore, magnetic and semiconducting character make these materials useful to spintronics and magneto-electronic devices while high Seebeck coefficient and thermoelectric figure of merit make them useful for the power generators and the Peltier cooling devices [3]. Furthermore, because wide band gap semiconducting materials permit devices to operate at much higher voltages, frequencies, and temperature than conventional semiconducting materials, hence these materials can also be suitable as a new alternate of other conventional semiconducting materials. $TlGdX_2$ (X = S, Se, Te) crystallize in the rhombohedral α-$NaFeO_2$ type structure (with space group $R-3m$, 166) belonging to the class of layered structure in which layers of magnetic ions are separated by three layers of nonmagnetic ions [4].

From literature point of view, $TlGdSe_2$ and $TlGdTe_2$ are first synthesized from their respective elements by heating method and then temperature dependent thermoelectric properties(Viz. the Seebeck coefficient, electrical conductivity and thermoelectric figure of merit) of these compounds were studied by Sankar et al. [3]. Thallium gadolinium dichalcogenides were also synthesized and structural, magnetic properties have been studied by Duczmal et al. [4–6]. Guseinov et al. studied many physical properties of similar type thallium rare earth dichalcogenides viz. $T1LuSe_2$, $T1YbSe_2$, $T1TmSe_2$, $T1ErSe_2$, $T1HoSe_2$, $T1DySe_2$, $T1TbSe_2$, $T1SmSe_2$, $T1GaSe_2$, $TlInSe_2$ [7]. To the best of our knowledge, a little study was made on these dichalcogenides. Thus, thallium gadolinium dichalcogenides have been preferred for first principle study on electronic, magnetic, thermodynamic and transport properties. First principle study on these materials will help in further understanding and controlling the material properties.

2. Computational method

Spin polarized electronic calculations were performed in terms of band structure and density of state histograms for spin up and spin down channel within density functional theory (DFT) using an accurate full potential linearized augmented plane-wave plus local orbital method (FPLAPW +LO) having generalized gradient approximations (GGA) implemented in WIEN2k package [8–10]. In this method the space is divided into non-overlapping muffin-tin (MT) spheres separated by an interstitial region. The basis functions are expanded into spherical harmonic functions inside the muffin-tin sphere and the Fourier series in the interstitial region. The k and E convergences were checked by increase of the number of k points and energy convergences criteria. The cutoff

*corresponding author; e-mail: rishisingh79@gmail.com

energy which defines the separation of valence and core states was chosen as –6.0 Ry. In the irreducible part of the Brillouin zone, $15 \times 15 \times 15$ k points were used to calculate the total and partial density of states. The self-consistent calculations were considered to be converged until the integrated charge difference between the last two iterations was less than $0.0001e$. The muffin tin sphere radii (RMT) for each atom of $TlGdX_2$ are taken as 2.5 for Tl and Gd in each case and 2.21 for Se, 2.48 for Se, and 2.50 for Te. The Fermi energies for $TlGdS_2$, $TlGdSe_2$, and $TlGdTe_2$ are found to be 0.2864, 2976, and 0.3129 eV, respectively.

The magnetic properties have been calculated in terms of magnetic moment and electron spin polarization. Electron spin polarization (P) identifies the type of magnetic materials viz. zero value of P shows paramagnetic/antiferromagnetic character of materials even below the magnetic transition temperature. The finite value of P indicates the ferromagnetic material below the Curie temperature. The electrons at E_{F} are fully spin polarized ($P = 100\%$) when $D_{\uparrow}(E_{\mathrm{F}})$ or $D_{\downarrow}(E_{\mathrm{F}})$ equals to zero [11–13].

The electron spin polarization at the Fermi energy (E_{F}) for a material can be calculated by the equation [11–13]:

$$P = \frac{D_{\uparrow}(E_{\mathrm{F}}) - D_{\downarrow}(E_{\mathrm{F}})}{D_{\uparrow}(E_{\mathrm{F}}) + D_{\downarrow}(E_{\mathrm{F}})}, \tag{1}$$

where $D_{\uparrow}(E_{\mathrm{F}})$ and $D_{\downarrow}(E_{\mathrm{F}})$ are the density of states for majority and minority spin channel at the Fermi level. Here, $\uparrow$ and $\downarrow$ denote the spin up and spin down.

Quasi-harmonic Debye model implemented in the Gibbs package [14, 15] was used to calculate thermodynamical behavior of $TlGdX_2$ (X = S, Se, Te). In quasi-harmonic Debye model the non-equilibrium Gibbs function $G^*(V;P,T)$ is in the form of

$$G*(V;P,T) = E(V) + PV + A_{vib}(\theta(V);T). \tag{2}$$

Here $E(V)$ is total energy per unit cell of $TlGdX_2$, P_V denotes the constant hydrostatic pressure, $\theta(V)$ is the Debye temperature, and A_{vib} is the vibration term which can be expressed using the Debye model of the phonon density of states as [14, 15]:

$$A_{vib}(\theta,T) = nkT \times \left(\frac{9\theta}{8T} + 3\ln\left(1 - \mathrm{e}^{-\theta/T}\right) - D\left(\theta/T\right)\right). \tag{3}$$

Here, n is the number of atoms per formula unit, $D(\theta/T)$ is the Debye integral. For an isotropic solid, θ can be expressed as [14, 15]:

$$\theta_{\mathrm{D}} = \frac{\hbar}{k}\sqrt[3]{6\pi n\sqrt{V}}f(\sigma)\sqrt{\frac{B_s}{M}}. \tag{4}$$

Here, M is the molecular weight per unit cell and B_s is the adiabatic bulk modulus, which is nearly equal to the static compressibility given by

$$B_s = B(V) = V\frac{\mathrm{d}^2E(V)}{\mathrm{d}V^2}. \tag{5}$$

$f(\sigma)$ is given by

$$f(\sigma) = \sqrt[3]{\frac{3}{2\sqrt{\left[\frac{2(1+\sigma)}{3(1-2\sigma)}\right]^3} + \sqrt{\left[\frac{1+\sigma}{3(1-\sigma)}\right]^3}}}. \tag{6}$$

The non-equilibrium Gibbs functions as a function of $(V;P,T)$ is minimized with respect to volume V:

$$\left.\frac{\partial G*(V;P,T)}{\partial V}\right|_{P,T} = 0. \tag{7}$$

By solving the above equation with respect to volume V, one can obtain the thermal equation of state(EOS) $V(P,T)$. The specific heat at constant volume and pressure (C_v, C_p) and thermal expansion coefficient α by using the expressions [14, 15]:

$$C_v = 3nk\left(4D\left(\theta/T\right) - \frac{3\theta/T}{\mathrm{e}^{\theta/T} - 1}\right), \tag{8}$$

$$S = nk\left(4D\left(\theta/T\right) - 3\ln(\mathrm{e}^{\theta/T} - 1)\right), \tag{9}$$

$$\alpha = \frac{\gamma C_v}{B_T V}, \tag{10}$$

$$C_p = C_v(1 + \alpha\gamma T). \tag{11}$$

Here γ represents the Grüneisen parameter, expressed as

$$\gamma = -\frac{\mathrm{d}\ln\theta(V)}{\mathrm{d}\ln V}. \tag{12}$$

Using optimized self-consistent field (SCF) calculations from WIEN2k, one can calculate the thermoelectric transport properties using the standard semiclassical Boltzmann theory in conjunction with rigid band approximation. All the calculations of the transport properties were implemented in the BoltzTrap package [16]. The electrical conductivity and the Seebeck coefficient tensors as a function of temperature T and chemical potential μ (near the Fermi energy) are expressed as

$$\sigma_{\alpha\beta}(T;\mu) = \frac{1}{\Omega}\int -\sigma_{\alpha\beta}(\varepsilon)\frac{\partial f_{\mu}(T;\mu)}{\partial\varepsilon}\,\mathrm{d}\varepsilon, \tag{13}$$

$$S_{\alpha\beta}(T;\mu) = \frac{1}{eT\Omega\sigma_{\alpha\beta}(T;\mu)} \times \int -\sigma_{\alpha\beta}(\varepsilon)(\varepsilon-\mu)\frac{\partial f_{\mu}(T;\mu)}{\partial\varepsilon}\,\mathrm{d}\varepsilon. \tag{14}$$

Here

$$\sigma_{\alpha\beta}(\mu) = \frac{e^2}{N}\sum_{i,k}\tau_{i,k}\upsilon_{\alpha}(i,k)\upsilon_{\beta}(i,k)\delta(\varepsilon - \varepsilon_{i,k}),$$

where α and β are tensor indices, e is the electronic charge, Ω is volume of unit cell, $\varepsilon(k)$ is the band energy, N is the number of k-points sampled, $\upsilon(k)$ is band velocity, $\tau(k)$ is the relaxation time and f is the Fermi function. In order to obtain accurate transport properties, the Brillouin zones of the unit cells were represented by the Monkhorst–Pack special k-point scheme [17] with $15 \times 15 \times 15$ grid meshes. Since τ cannot be determined from band structure calculations, thus in our approach the relaxation time is assumed to be a constant, based on the consideration that the electrons contributing to transport are in a narrow energy range due to the delta-function like the Fermi broadening. The relaxation time

is nearly the same for the electrons in such a narrow energy range [18].

3. Results and discussion

3.1. Structural properties

The structural parameters viz. lattice parameters, bulk modulus and its first order pressure derivative have been estimated through fitting the total energy data with the Murnaghan equation of state [19] given by

$$E_{tot} = E_0(V) + \frac{B_0 V_0}{B_0' B_0' - 1)} \times \left[B_0 \left(1 - \frac{V_0}{V}\right) + \left(\frac{V_0}{V}\right)^{B_0'} - 1 \right], \quad (15)$$

where E_0 and V_0 are the energy and volume at equilibrium, B_0 and B_0' are the equilibrium bulk modulus and its first order pressure derivative.

TABLE I

Lattice parameters, a_0, c_0 (Å), bulk modulus, B_0 [GPa] and pressure derivative of bulk modulus, B_0' in equilibrium condition for $TlGdS_2$, $TlGdSe_2$, $TlGdTe_2$ using GGA.

	$TlGdS_2$	$TlGdSe_2$	$TlGdTe_2$
a_0, c_0	4.026, 22.29	4.131, 23.01	4.403, 24.20
exp. [3, 4]	4.048, 22.40	4.183, 23.08	4.428, 24.25
B_0	52.97	44.70	35.95
B_0'	4.11	4.21	4.03

The calculated lattice parameters a_0, c_0, bulk modulus B_0 and its first order pressure derivative B_0' are shown in Table I. Calculated values of lattice parameters show good agreement with experimental values [3, 4]. Bulk modulus B_0 is a material property indicating the degree of resistance of a material to compression. The larger the bulk modulus, the greater is the degree of resistance. It can be observed from Table I that $B_{TlGdS_2} > B_{TlGdSe_2} > B_{TlGdTe_2}$ which indicates that degree of resistance decreases from $TlGdS_2 \rightarrow TlGdSe_2 \rightarrow TlGdTe_2$.

The energy (E_0) versus volume (V_0) curves (which indicate the stability of the material) for $TlGdS_2$, $TlGdSe_2$ and $TlGdTe_2$ are illustrated in Fig. 1a–c, respectively. It is clear from theses figures that all the three compounds are stable with equilibrium energy values (E_0) –64736.1688, –72860.2376, and –90326.7967 eV at the equilibrium volume (V_0) 731.7552, 821.5613, and 995.5196 a.u.^{3} for $TlGdS_2$, $TlGdSe_2$, and $TlGdTe_2$, respectively. It is evident that equilibrium energy decreases while equilibrium volume increases from $TlGdS_2 \rightarrow TlGdSe_2 \rightarrow TlGdTe_2$. This indicates that the stability of the molecules increases with increase of the molecular weight from $TlGdS_2 \rightarrow TlGdSe_2 \rightarrow TlGdTe_2$. Its reason is that, as molecular weight increases, the molecule needs smaller volume to vibrate in the unit cell to occupy equilibrium state. As a result, equilibrium energy decreases and equilibrium unit cell volume increases from $TlGdS_2 \rightarrow TlGdSe_2 \rightarrow TlGdTe_2$ [20].

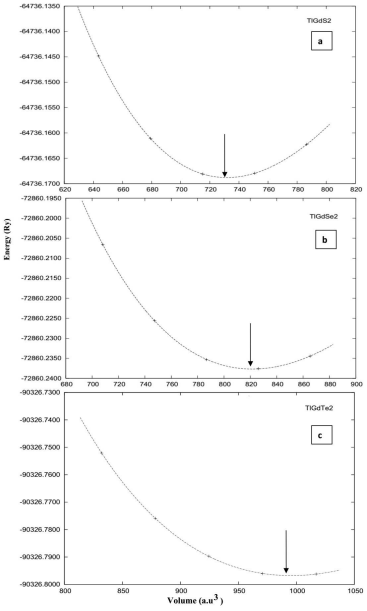

Fig. 1. Total energy as a function of unit cell volume for (a) $TlGdS_2$, (b) $TlGdSe_2$, (c) $TlGdTe_2$ with GGA approximation.

3.2. Spin polarized electronic and magnetic properties

Electronic behavior of $TlGdX_2$ has been shown in terms of energy bands and total, partial density of states. The calculated band structures along the high symmetry directions Γ, Δ, H, N, Σ, Λ, and P in the irreducible Brillouin zone for spin up and spin down channel for $TlGdS_2$, $TlGdSe_2$, and $TlGdTe_2$ were shown in Fig. 2a,b, 2c,d, and 2e,f, respectively. The different colors in Fig. 2a,b, 2c,d, and 2e,f show that the bands lie in different energy range along different symmetry directions Γ, Δ, H, N, Σ, Λ and P in the Brillouin zone for spin up and spin down channels. These figures indicate that most of the valence bands lie from –13.0 eV to 0.0 eV (where the Fermi level, E_F, is considered at origin). The band structure histograms of $TlGdS_2$, $TlGdSe_2$, and $TlGdTe_2$ for both the majority and minority channel confirm an indirect band gap, indicating that $TlGdS_2$, $TlGdSe_2$, and $TlGdTe_2$ are commonly semiconducting materials at its own equilibrium lattice constant. The band structure for spin down channel shows narrower band gap compared to the spin up channel for $TlGdX_2$ (X = S, Se, Te). This is due to presence of Gd f spin down channel at around 1.0 eV for $TlGdS_2$, $TlGdSe_2$, and 0.5 eV for $TlGdTe_2$. Furthermore, the effective indirect band gap is found to be 1.86, 1.36, and 0.48 eV for $TlGdS_2$, $TlGdSe_2$, and $TlGdTe_2$, respectively.

Total density of states (TDOS) and partial density of states (PDOS) plots for $TlGdS_2$, $TlGdSe_2$, and $TlGdTe_2$ have been shown in Figs. 3a–i, 4a–j, and 5a–j, respectively. In case of $TlGdS_2$, Fig. 3a depicts that there are mainly three peaks in the majority spin channel below the Fermi level at around –11.0, –4.0, and –2.0 eV. The

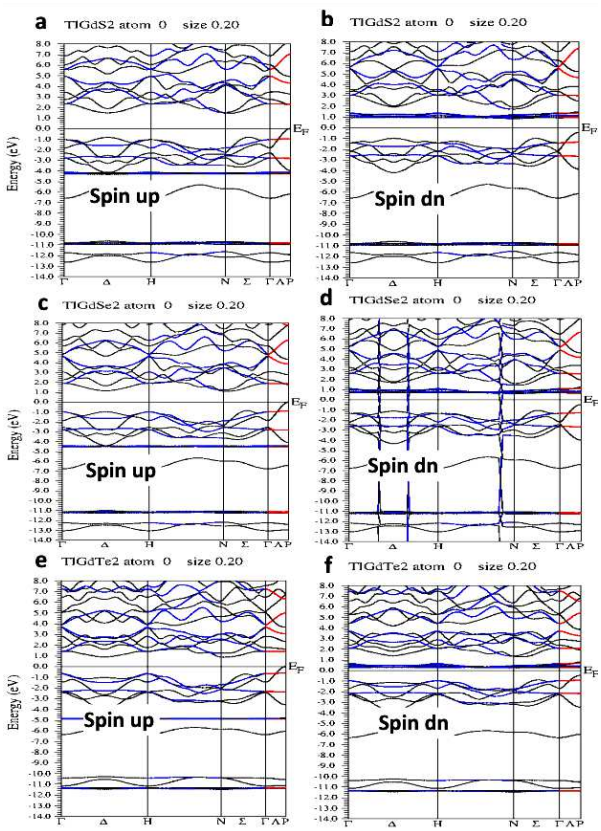

Fig. 2. Spin polarized electron dispersion curves along high symmetry directions in the Brillouin zone for (a) $TlGdS_2$ up, (b) $TlGdS_2$ down, (c) $TlGdSe_2$ up, (d) $TlGdSe_2$ up,(E) $TlGdTe_2$ up, (f) $TlGdTe_2$ up.

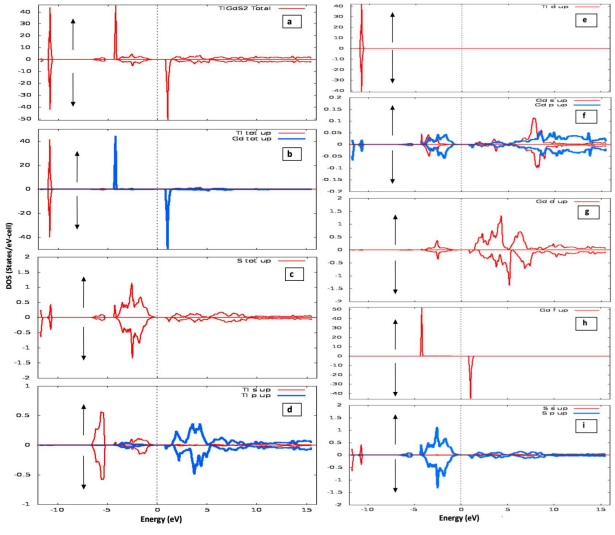

Fig. 3. Calculated total and partial density of states for (a) $TlGdS_2$ total, (b) Tl total and Gd total, (c) Se total, (d) Tl s and Tl p orbital,(E) Tl d orbital, (f) Gd s and Gd p orbital, (g) Gd d orbital, (h) Gd f orbital, (i) S s and S p orbital.

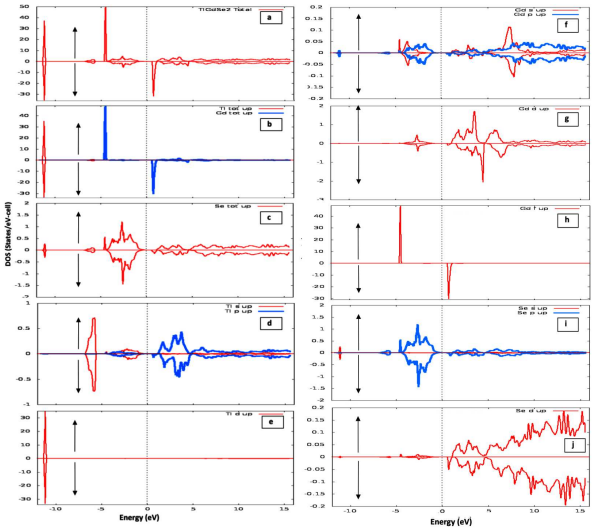

Fig. 4. Calculated total and partial density of states for (a) $TlGdSe_2$ total, (b) Tl total and Gd total, (c) Se total, (d) Tl s and Tl p orbital,(E) Tl d orbital, (f) Gd s and Gd p orbital, (g) Gd d orbital, (h) Gd f orbital, (i) Se s and Se p orbital, (j) Se d orbital.

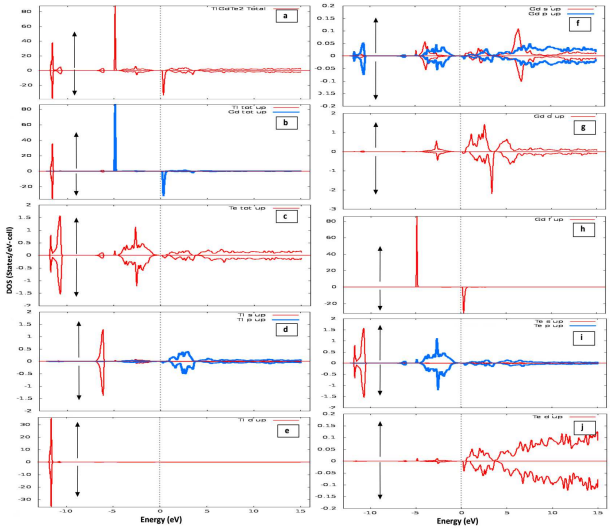

Fig. 5. Calculated total and partial density of states for (a) $TlGdTe_2$ total, (b) Tl total and Gd total, (c) Te total, (d) Tl s and Tl p orbital,(E) Tl d orbital, (f) Gd s and Gd p orbital, (g) Gd d orbital, (h) Gd f orbital, (i) Te s and Te p orbital, (j) Te d orbital.

peak at around –11.0 eV is due to mainly Tl d states (Fig. 3e). The sharp peak at around –4.0 eV is due to mainly Gd f states (Fig. 3h) with small contribution of Tl s (Fig. 3d) states of majority channel. The states at around –2.0 eV are due to hybridization of Tl s, Gd p, and S p states (Fig. 3d,f,i) of majority channels. For spin down, two peaks were observed in the minority spin channel below the Fermi level at around –11.0 eV and –2.0 eV. The DOS at around –11.0 eV is due to Tl d

states (Fig. 3e), whereas DOS at around –2.0 eV is due to hybridization of Tl s, Gd p and S p states (Fig. 3d,f,i). It is evident from Fig. 3a that minority spin channel of Gd f states are at around 1.0 eV which are responsible for the magnetic moment and for reducing the band gap in spin down channel as band gap is narrower for spin down compared to spin up channel. Almost, similar features of TDOS and PDOS for $TlGdSe_2$ and $TlGdTe_2$ have been obtained which are depicted in Fig. 4a–j and Fig. 5a–j and can be discussed in similar fashion.

TABLE II

Calculated spin magnetic moments [μ_B] of $TlGdS_2$, $TlGdSe_2$, and $TlGdTe_2$.

	$TlGdS_2$	$TlGdSe_2$	$TlGdTe_2$
interstitial region	0.1053	0.1109	0.1222
Tl	–0.0007	–0.0012	–0.0015
Gd	7.1096	7.0611	6.9012
S, Se, Te	–0.0061	–0.0081	–0.0108
total	7.0081	7.0083	7.0111
exp. [4]	7.85	7.75	–

The calculated and experimental values of total magnetic moments of $TlGdS_2$, $TlGdSe_2$, and $TlGdTe_2$ along with the magnetic moment in the interstitial region and at each atom have been shown in Table II. The values of calculated total magnetic moment of the $TlGdS_2$, $TlGdSe_2$, and $TlGdTe_2$ compounds are found to be 7.21, 7.17, and 7.01 μ_B which are in close agreement with the available experimental values 7.85 μ_B and 7.75 μ_B [4] for $TlGdS_2$, $TlGdSe_2$. From Table II, it can also be seen that total magnetic moment of $TlGdS_2$, $TlGdSe_2$, and $TlGdTe_2$ is mainly dominant by contribution of individual moments of Gd^{3+} ions.

The value of electron spin polarization at the Fermi energy (E_F) for a material is calculated by Eq. (1). In our case of $TlGdS_2$, $TlGdSe_2$, and $TlGdTe_2$ large view of TDOS depicts that value of $D_\uparrow(E_F)$ is very small (≈ 0.001 states/(eV cell)), while $D_\downarrow(E_F)$ vanishes at the Fermi level which gives $P = 1$ (i.e. $P = 100\%$), implying all the three compounds are ferromagnetic and nearly fully spin polarized.

3.3. Thermodynamic and transport properties

Quasiharmonic Debye model has been used successfully to calculate the temperature dependent thermodynamic properties of $TlGdX_2$ (X = S, Se, Te). The effect of temperature has been studied in a wide temperature range 0–600 K for $TlGdS_2$, 0–500 K for $TlGdSe_2$, and 0–180 K for $TlGdTe_2$.

Temperature variations of volume (V), bulk modulus (B), the Debye temperature (θ_D), the Grüneisen parameter (γ), specific heat (C_v) and thermal expansion coefficient, α for $TlGdX_2$ (X = S, Se, Te) are shown in Figs. 6–8. Figures 6a, 7a, and 8a demonstrate the temperature variation of unit cell volume (V) for $TlGdS_2$, $TlGdSe_2$, and $TlGdTe_2$, respectively, and indicate that unit cell

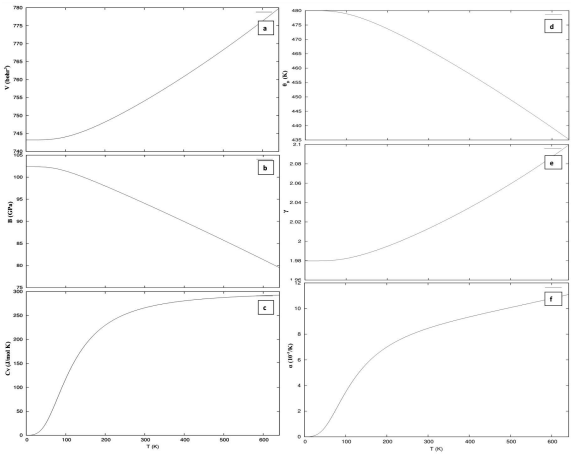

Fig. 6. Temperature induced variation in (a) volume V, (b) bulk modulus B, (c) specific heat C_V, (d) the Debye temperature θ_D, (E) the Grüneisen parameter γ, and (f) thermal expansion coefficient α for $TlGdS_2$.

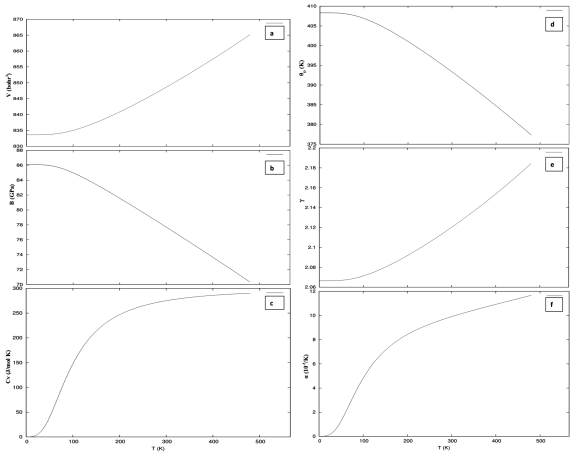

Fig. 7. As in Fig. 6 but for $TlGdSe_2$.

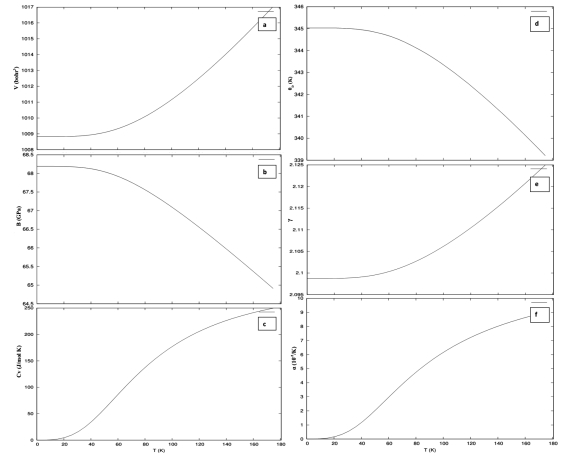

Fig. 8. As in Fig. 6 but for $TlGdTe_2$.

volume (V) increases with temperature. This increase in volume with temperature is due to the expansion of unit cell dimensions with temperature. Figures 6b, 7b, and 8b show that bulk modulus, B decreases with increase of the temperature. This decrease in bulk modulus with increase of the temperature is caused by change in unit cell volume with temperature. Value of B also provides an idea about the degree of resistance of $TlGdX_2$ (X = S, Se, Te) which decreases with increase of the temperature, signifying that materials become softer with increase of the temperature. The temperature dependent behavior of the calculated heat capacity at constant volume (C_v) is shown in Figs. 6c, 7c, and 8c for $TlGdS_2$, $TlGdSe_2$, and $TlGdTe_2$, respectively.

These figures show that C_V increases with the temperature up to $T \approx 300$ K for $TlGdS_2$, $TlGdSe_2$, and $T \approx 160$ K for $TlGdTe_2$ (follows the Debye T^3 law) and at temperature $T > 300$ K for $TlGdS_2$, $TlGdSe_2$, and $T > 160$ K for $TlGdTe_2$, C_v approaches to a constant value (the Dulong–Petit limit), indicating that the temperature has small impact for $TlGdS_2$ and $TlGdSe_2$ while larger impact for $TlGdTe_2$ on the heat capacity at constant volume. Figures 6d, 7d, and 8d display the variation of the Debye temperature (θ_D) with temperature which point out that θ_D decreases at slow rate with increase of temperature for $TlGdX_2$ (X = S, Se, Te). The slow variation in θ_D with increase of the temperature reflects small effect of temperature on θ_D. In case of $TlGdX_2$ (X = S, Se, Te), the slow variation of θ_D with temperature also reflects the fact that the thermal vibration frequency of the atoms in $TlGdX_2$ (X = S, Se, Te) changes slowly with the temperature.

TABLE III

Calculated energy gap E_g [eV], the Fermi energy E_F [eV], the Debye temperature θ_D [K], the Grüneisen parameter γ, thermal expansion coefficient α [10^{-5}/K], specific heat C_V [J/(mol K)] in equilibrium condition for $TlGdS_2$, $TlGdSe_2$, and $TlGdTe_2$ using GGA.

	$TlGdS_2$	$TlGdSe_2$	$TlGdTe_2$
E_g	1.863	1.362	0.488
E_F	0.3510	0.3542	0.3935
θ_D	465	393	317
γ	2.01	2.12	2.13
α	7.80	9.80	10.20
C_V	260	255	250

Further, it can be observed from Table III that θ_D decreases from $TlGdS_2 \rightarrow TlGdSe_2 \rightarrow TlGdTe_2$, reflecting that thermal vibrational frequency decreases from $TlGdS_2 \rightarrow TlGdSe_2 \rightarrow TlGdTe_2$. Figures 6e, 7e, and 8e depict the variation of the Grüneisen parameter, γ (which is measure of anharmonicity of the lattice) [21], with temperature and show that γ increases with temperature, indicating that anharmonicity increases with temperature. Figures 6f, 7f, and 8f show the variation of thermal expansion coefficient, α, as a function of temperature. The thermal expansion coefficient increases rapidly especially in the temperature range $< 0T < 300$ K for $TlGdS_2$ and $TlGdSe_2$ and $0 < T < 180$ K for $TlGdTe_2$, indicating that temperature has high impact on thermal expansion coefficient, α.

The standard semiclassical Boltzmann theory was used to calculate the transport properties in terms of the Seebeck coefficients (S) and electrical conductivity (σ) for $TlGdX_2$ (X = S, Se, Te). The Seebeck coefficient of a material is the measure of the magnitude of an induced thermoelectric voltage in response to a temperature difference across that material. The Seebeck coefficient may be negative and positive. Negative value of S indicates that charged carriers are negative (like electrons), and positive value of S indicates that charged carriers are positive (like holes). The materials that have zero Seebeck coefficients are known to be superconductors. Even though metals have large amount of carriers, they have been known to have smaller Seebeck coefficient values due to their large electronic contribution to the thermal conductivity. Semiconductors are known to have larger Seebeck coefficient values because they can have large amount of carrier like metals but have low thermal conductivity. The ideal semiconductors have large Seebeck coefficient, low thermal conductivity, and high electrical conductivity [22, 23].

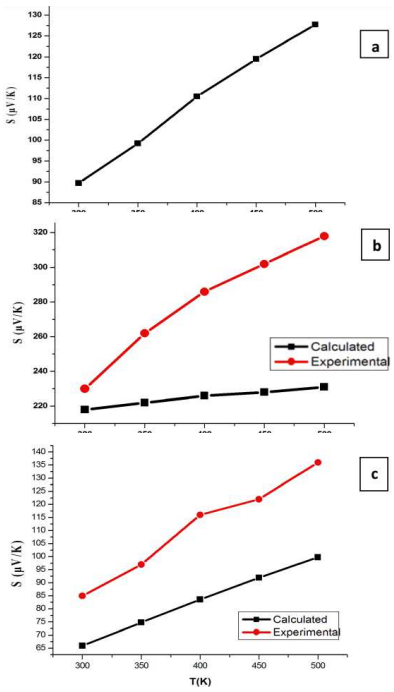

Fig. 9. Temperature induced variation in the Seebeck coefficient (S) for (a) $TlGdS_2$, (b) $TlGdSe_2$, (c) $TlGdTe_2$.

The calculated and experimental values of the Seebeck coefficient S and electrical conductivity σ for the $TlGdX_2$ (X = S, Se, Te) compounds at about room temperature have been displayed in Table IV. The calculated values of S were found to be about 90, 218, and 66 μV/K

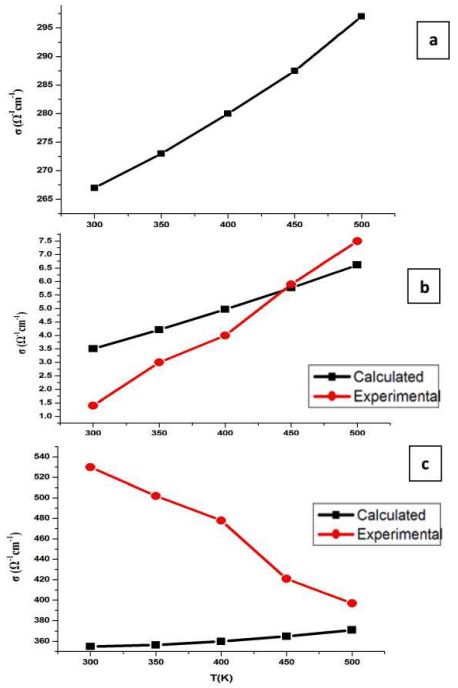

Fig. 10. Temperature induced variation in electrical conductivity (σ) for (a) $TlGdS_2$, (b) $TlGdSe_2$, (c) $TlGdTe_2$.

TABLE IV

Seebeck coefficient S [μV/K] and electrical conductivity, σ [Ωcm^{-1}] at 300 K for $TlGdS_2$, $TlGdSe_2$, and $TlGdTe_2$.

	$TlGdS_2$	$TlGdSe_2$	$TlGdTe_2$
S	89	218	65
exp. [3]	–	230	85
σ	267	3.51	355
exp. [3]	–	1.40	530

for $TlGdS_2$, $TlGdSe_2$, and $TlGdTe_2$, respectively, which are consistent with the available experimental value [3] 230 μ V/K for $TlGdSe_2$ and 85 μ V/K for $TlGdTe_2$. The calculated values of σ were found to be about 267, 3.51, and 355 Ωcm^{-1} for $TlGdS_2$, $TlGdSe_2$, and $TlGdTe_2$, respectively, which are also found to be consistent with the available experimental values [3] 1.40 Ωcm^{-1} for $TlGdSe_2$ and 530 Ωcm^{-1} for $TlGdTe_2$. The temperature variation of calculated values of S has been depicted in Fig. 9a–c for $TlGdS_2$, $TlGdSe_2$, and $TlGdTe_2$, respectively, in temperature range 300–500 K. The experimental values of S for $TlGdS_2$ are not available in the literature, only for $TlGdSe_2$ and $TlGdTe_2$ are available. Therefore, temperature variation of experimental values of S has also been shown along with calculated values for $TlGdSe_2$ and $TlGdTe_2$ in Fig. 9b and c. These calculated and experimental values are found to be in good agreement.

Temperature variation of calculated values of electrical conductivity (σ) has been shown in Fig. 10a–c for $TlGdS_2$, $TlGdSe_2$, and $TlGdTe_2$, respectively. The experimental values of σ are available only for $TlGdSe_2$ and $TlGdTe_2$ [3], which are depicted along with calculated values in Fig. 10b and c. From Fig. 10b and c, one can see that calculated values of σ for $TlGdSe_2$ show good agreement with experimental values. But in case of $TlGdTe_2$, experimental values show decreasing nature with temperature whereas our calculated values show increasing nature with temperature. This may be due to large contribution of electrical conductivity with respect to temperature and small contribution of thermal conductivity in semiconductors.

4. Conclusions

Full potential linearized potential augmented plane wave method along with GGA, quasiharmonic Debye model, and semiclassical Boltzmann model has been used to study the electronic, thermodynamic, and transport properties of thallium gadolinium dichalcogenides ($TlGdX_2$, X = S, Se, Te). Our calculated values of structural parameters are in good agreement with experimental/theoretical values. These dichalcogenides show the semiconducting nature with indirect wide band gaps 1.86, 1.36, and 0.48 eV for $TlGdS_2$, $TlGdSe_2$, and $TlGdSe_2$, respectively. In the total density of states and partial density of states plots, minority spin channel of Gd f states are dominant above the Fermi level at around 1.0 eV which are responsible for the magnetic moment and for reducing the band gap in spin down channel. The calculated total magnetic moment of the $TlGdS_2$, $TlGdSe_2$, and $TlGdTe_2$ compounds are found in close agreement with the available experimental values and total magnetic moment is mainly dominant by contribution of individual moments of Gd^{3+} ions. Decreasing value of θ_D from $TlGdS_2 \rightarrow TlGdSe_2 \rightarrow TlGdTe_2$, indicate that thermal vibrational frequency decreases from $TlGdS_2 \rightarrow TlGdSe_2 \rightarrow TlGdTe_2$. The calculated values of S and σ are found to be in good agreement with the experimental values.

References

[1] J.K. Furdyna, *J. Appl. Phys.* **64**, R29 (1988).

[2] H. Ohno, *Science* **281**, 951 (1998).

[3] C.R. Sankar, S.B. Sanasy, H. Kleinke, *J. Electron. Mater.* **41**, 1662 (2012).

[4] M. Duczmal, L. Pawlak, S. Pokrzywnicki, *Acta Phys. Pol. A* **97**, 839 (2000).

[5] M. Duczmal, L. Pawlak, *J. Alloys Comp.* **225**, 181 (1995).

[6] M. Duczmal, L. Pawlak, *J. Alloys Comp.* **219**, 189 (1995).

[7] G.D. Guseinov, G.B. Abdullayev, S.M. Bidzinova, F.M. Seidov, M.Z. Ismailov, A.M. Pashayev, *Phys. Lett.* **33A**, 421 (1970).

[8] K. Schwarz, P. Blaha, *Comput. Mater. Sci.* **28**, 259 (2003).

[9] P. Blaha, K. Schwarz, G.K.H. Madsen, D. Kvasnicka, J. Luitz, *WIEN2k, An augmented plane wave plus local orbitals program for calculating crystal properties*, Technical University, Austria 2001.

[10] G.K.H. Madsen, P. Blaha, K. Schwarz, E Sjöstedt, L Nordström, *Phys. Rev. B* **64**, 195134 (2001).

[11] R.J. Soulen Jr., J.M. Byers, M.S. Osofsky, B. Nadgorny, T. Ambrose, *Science* **282**, 85 (1998).

[12] D.P. Rai, R.K. Thapa, *Chin. J. Phys.* **51**, 812 (2013).

[13] H.C. Kandpal, G.H. Fecher, C. Felser, *J. Phys. D Appl. Phys.* **40**, 1507 (2006).

[14] M.A. Blanco, E. Francisco, *Comput. Phys. Commun.* **158**, 57 (2004).

[15] A. Otero-de-la-Roza, D. Abbasi-Pérez, V. Luaña, *Comput. Phys. Commun.* **182**, 2232 (2011).

[16] G.K.H. Madsen, D.J. Singh, *Comput. Phys. Commun.* **175**, 67 (2006).

[17] H.J. Monkhorst, J.D. Pack, *Phys. Rev. B* **13**, 5188 (1976).

[18] P. Hua, W. Chun-Lei, Li Ji-Chao, Z. Rui-Zhi, W. Hong-Chao, S. Yi, *Chin. Phys. B* **20**, 046103 (2011).

[19] F.D. Murnaghan, *Proc. Natl. Acad. Sci. U.S.A.* **30**, 244 (1944).

[20] R.P. Singh, *Ind. J. Phys.* **89**, 377 (2015).

[21] R.K. Singh, R.P. Singh, M.P. Singh, *Physica B* **404**, 95 (2009).

[22] T.C. Harman, P.J. Taylor, M.P. Walsh, B.E. Laforge, *Science* **297**, 2229 (2002).

[23] A. Ishida, T. Yamada, T. Nakano, Y. Takan, S. Takaoka, *Jpn. J. Appl. Phys.* **50**, 031302 (2011).